BUTTERWORTH HEINEMANN

Recirculating laminar mixed convection in a horizontal parallel plate duct

D. B. Ingham and P. Watson
Department of Applied Mathematical Studies, The University of Leeds, Leeds, UK

P. J. Heggs
Department of Chemical Engineering, University of Manchester Institute of Science and Technology, Manchester, UK

Numerical investigations are conducted into steady, two-dimensional (2-D), laminar combined convection flows bounded between two very long and wide horizontal parallel plates. At some location along the duct, one, or both, of the duct surfaces undergoes a temperature change. These temperature changes create three case studies; namely, the lower wall is heated, the upper wall is heated, and both walls are heated. Results are obtained for a fixed Prandtl number of 7.02 at low and moderate values of the Reynolds number over a wide range of values for the ratio of the Grashof number to the square of the Reynolds number. It is observed that when applying heat at the upper wall, a thermally stratified flow is generated, and when the fluid is heated from the lower wall, a transversely oriented recirculation is predicted that extends upstream of the wall temperature discontinuity for values of $Gr/Re^2 > 17$; the exact value is a function of Re. When applying heat on both walls simultaneously, the stratification and recirculation effects of the other two cases are combined and enhanced.

Keywords: mixed convection; recirculation; parallel plate duct; local Nusselt numbers; friction factors

Introduction

Laminar convection in internal flows has been the subject of much theoretical and experimental research, and a thorough literature survey has been given by Aung (1987). The area of combined laminar convection is of great importance because of its wide ranging engineering applications; e.g., in the cooling processes in the primary and secondary circuits of nuclear reactors, heat transfer processes in the design and control of compact heat exchangers, the flow of cement or muds in bore holes during drilling and cementing operations in the gas and oil industries, and in the cooling of densely packed circuit cards in electronic equipment.

The results of numerous experimental and numerical investigations concerned with free convection effects on forced flow laminar heat transfer within horizontal ducts are available in the literature. Mori and Uchida (1966) performed an experimental and theoretical study on the effect of buoyancy-generated vortex rolls that align parallel to the streamwise direction in fully developed forced convection heat transfer between horizontal parallel plates, where the lower plate was hot and the upper plate was cold. The conditions specifying the onset of longitudinal Görtler vortices was also studied analytically by Nakayama et al. (1970) and then Akiyama et al. (1971) reproduced the phenomena experimentally using air as the working fluid. Buoyancy effects on the heat transfer in a thermally developing horizontal parallel plate duct for the case of heating from below and above with unequal uniform heat fluxes was investigated experimentally by Osborne and Incropera (1985). Heating from above produced thermal stratification of the upper boundary layer, which was virtually impenetrable to the buoyancy-induced secondary flow originating from the heated lower plate.

The influence of the buoyancy force on laminar forced convection in the entrance region between horizontal parallel plates was studied by Naito (1984) when either, or both, of the walls of the duct are maintained at equal constant temperatures or where one wall is held at a constant temperature, and the opposite wall is insulated. The onset of heating coincided with the duct inlet, where the flow velocity was uniform. In terms of the parameters defined in this paper, the maximum value of the ratio of the buoyancy force to the intertia force used by Naito was 5.63, and this was found to be insufficient to produce recirculating flows. Naito and Nagano (1989) generalized the earlier research of Natio to inclined parallel plates.

Address reprint requests to Professor P. J. Heggs, Department of Chemical Engineering, UMIST, P.O. Box 88, Manchester, M60 1QD, UK.

Received 17 November 1992; accepted 12 January 1995

Int. J. Heat and Fluid Flow 16: 202–210, 1995

0142-727X/95/$10.00
SSDI 0142-727X(95)00014-H

In this paper, the combined convection between two horizontal parallel plates is investigated numerically for low and moderate values of the Reynolds number, so that the terms representing the streamwise diffusion of momentum and energy must be retained. The governing equations of mass, momentum, and energy retain their respective coupling and nonlinearity in the advection of momentum and heat. Hence, changing the duct wall temperature affects both the fluid and thermal fields. The governing parameters of this problem are the Reynolds number Re, the Prandtl number Pr, and the ratio of the Grashof number to the square of the Reynolds number Gr/Re^2. The range of values of the parameter Gr/Re^2 is selected to encompass both pure forced convection and large-scale recirculating flows generated when the fluid is heated from below. These low-to-moderate Reynolds number flows are computed with a Grashof number that is associated with heat and fluid flow in the laminar regime. The numerical method selected for the problem is similar to the technique used by Morton et al. (1989), although a variety of higher-order approximations, such as the QUICK scheme, were tried, but they yielded oscillating solutions near to the temperature discontinuity.

Governing equations and numerical model

In the industries mentioned in the introduction, there are many situations when a Newtonian fluid of constant temperature flows along a very long and wide duct. Then, at some location along the duct, the temperature of one, or both, of the walls of the duct changes rapidly to another constant temperature. This physical situation is mathematically modeled as a steady, laminar combined convection of a viscous fluid, with velocity components u, v, which is confined between two very wide horizontal parallel plates, which mathematically may be modeled between two very wide horizontal parallel plates; i.e., the fluid flow takes place in the domain $-\infty < x < \infty$, $-a \le y \le a$, and the temperature changes at $x = 0$. In the far upstream region ($x \to -\infty$), the fluid is in fully developed Poiseuille flow and is at a constant temperature T_e. At the duct exit ($x \to \infty$), fully developed Poiseuille flow is attained, and the temperature profile becomes either constant or a linear function of y.

Three thermal temperature boundary conditions are considered as follows:

Case I: Heated lower wall:

$$\begin{aligned} T &= T_e \quad \text{for} \quad -\infty < x < 0 \quad y = -a \\ T &= T_h \quad \text{for} \quad 0 \le x < \infty \quad y = -a \\ T &= T_e \quad \text{for} \quad -\infty < x < \infty \quad y = +a \end{aligned} \tag{1}$$

Case II: Heated upper wall:

$$\begin{aligned} T &= T_e \quad \text{for} \quad -\infty < x < \infty \quad y = -a \\ T &= T_e \quad \text{for} \quad -\infty < x < 0 \quad y = +a \\ T &= T_h \quad \text{for} \quad 0 \le x < \infty \quad y = +a \end{aligned} \tag{2}$$

Case III: Heated lower and upper walls:

$$\begin{aligned} T &= T_e \quad \text{for} \quad -\infty < x < 0 \quad y = \pm a \\ T &= T_h \quad \text{for} \quad 0 \le x < \infty \quad y = \pm a \end{aligned} \tag{3}$$

For Case I (and Case III to a lesser extent), the fluid flow will be unstable under certain operating conditions caused by the top heavy density distribution caused by the heating from below (see Mori and Uchida 1966 and Hwang and Cheng 1973). However, before a stability analysis can be performed then the steady solution must first be determined, and, hence, the importance of the present investigation. Even in circumstances where instabilities arise, the predictions of this analysis will be appropriate up to the location where instabilities first occur.

The working fluid is assumed to be Newtonian with constant specific heat capacity, coefficient of expansion, thermal conductivity, and dynamic viscosity. The gravity force acts vertically downward in the negative y-direction perpendicular to the surfaces of the duct, the Boussinesq approximation is invoked, and viscous dissipation is neglected, because it has only a small effect (see Collins 1975). The above assumptions were designed to keep the theoretical model as simple as possible, although including variations in the physical quantities, such as temperature-dependent viscosity, present no difficulties in the mathematical formulation (see Collins 1980).

Notation

a	half duct width
b	streamwise location corresponding to the computational duct inlet
c_p	specific heat capacity at constant pressure
f	friction factor
g	acceleration due to gravity
Gr	Grashof number, $= g\beta(T_h - T_e)a^3/\nu^2$
h	local heat transfer coefficient
k	thermal conductivity of the fluid
L	dimensionless streamwise length
Nu	local Nusselt number, $= ha/k$
Q	mass flux of fluid
p	fluid pressure
P	dimensionless pressure, $= (p - p_e + g\rho_e y)/\rho_e u_m^2$
Pr	Prandt number, $= \nu/\alpha$
Re	Reynolds number, $= au_m/\nu$
T	temperature
u, v	streamwise and transverse velocity components
U, V	dimensionless streamwise and transverse velocities, $= u/u_m$ and v/u_m
x, y	streamwise and transverse coordinates
X, Y	dimensionless streamwise and transverse coordinates, $= x/a\text{Re}$ and y/a

Greek

α	molecular thermal diffusivity
β	coefficient of expansion, $= (-1/\rho)(\partial\rho/\partial T)$
θ	dimensionless temperature
ρ	fluid density
ψ	dimensionless stream function
ω	kinematic viscosity
Ω	dimensionless vorticity

Subscripts

d	upstream flow region
e	value taken at duct entrance
h	value taken at the hot wall
L	upper wall value
m	mean value
u	upstream flow region
U	upper wall value
∞	value taken at infinity

The fluid and thermal fields within a horizontal two-dimensional (2-D) parallel walled duct are governed by the equations of continuity, streamwise and transverse momentum and energy, which can be written in the following form:

$$\frac{\partial u}{\partial x} + \frac{\partial v}{\partial y} = 0 \tag{4}$$

$$u\frac{\partial u}{\partial x} + v\frac{\partial u}{\partial y} = -\rho_e^{-1}\frac{\partial p}{\partial x} + \nu\left\{\frac{\partial^2 u}{\partial x^2} + \frac{\partial^2 u}{\partial y^2}\right\} \tag{5}$$

$$u\frac{\partial v}{\partial x} + v\frac{\partial v}{\partial y} = -\rho_e^{-1}\frac{\partial p}{\partial y} + \nu\left\{\frac{\partial^2 v}{\partial x^2} + \frac{\partial^2 v}{\partial y^2}\right\} - g[1 - \beta(T - T_c)] \tag{6}$$

$$\left\{u\frac{\partial T}{\partial x} + v\frac{\partial T}{\partial y}\right\} = \alpha\left\{\frac{\partial^2 T}{\partial x^2} + \frac{\partial^2 T}{\partial y^2}\right\} \tag{7}$$

It is assumed that the flow and temperature of the fluid in the duct do not feel the effects of the change in the temperature boundary condition at $x = 0$ before the location $x = -b$. The value of b is adjusted in each calculation so that any larger value of b causes no change in any of the results presented in this paper. Thus, the boundary conditions for Case I—the fluid being heated from the lower wall— are as follows:

at

$$x = -b, \quad -a \le y \le a, \quad u = u_e, \quad v = 0, \quad T = T_c \tag{8}$$

at

$$x \to \infty, \quad -a \le y \le a, \quad u \to u_f, \quad v \to 0, \quad T \to T(y) \tag{9}$$

at

$$y = -a, \quad \begin{matrix} -b \le x < \infty, & u = 0, & v = 0 \\ -b \le x < 0, & T = T_c & \\ 0 \le x < \infty, & T = T_h & \end{matrix} \tag{10}$$

at

$$y = a, \quad -b \le x < \infty \quad u = 0, \quad v = 0, \quad T = T_c \tag{11}$$

The velocity $u_e = u_f$ corresponds to the fully developed parabolic profile, and $T(y)$ is a linear function of y. The boundary conditions for Cases II and III differ only in the wall temperature definitions as specified in Equations 2 and 3, respectively.

The following dimensionless variables:

$$X = x/a\mathrm{Re}, \; Y = y/a, \; U = u/u_m, \; V = v/u_m,$$

$$P = (p - p_e + g\rho_e y)/\rho_e u_m^2 \quad \text{and} \quad \theta = (T - T_c)/(T_h - T_c) \tag{12}$$

are now introduced. On introducing the stream function $\psi(X, Y)$, which satisfies the continuity Equation 4 defined by the following:

$$U = \frac{\partial \psi}{\partial Y}, \qquad V = -\mathrm{Re}^{-1}\frac{\partial \psi}{\partial X} \tag{13}$$

then the dimensionless vorticity can be written as follows:

$$\Omega = -\left\{\frac{1}{\mathrm{Re}^2}\frac{\partial^2 \psi}{\partial X^2} + \frac{\partial^2 \psi}{\partial Y^2}\right\} \tag{14}$$

Eliminating the pressure terms in the momentum Equations 5 and 6 results in the following stream function–vorticity formulation:

$$\frac{\partial \Omega}{\partial X}\frac{\partial \psi}{\partial Y} - \frac{\partial \psi}{\partial X}\frac{\partial \Omega}{\partial Y} = \frac{1}{\mathrm{Re}^2}\frac{\partial^2 \Omega}{\partial X^2} + \frac{\partial^2 \Omega}{\partial Y^2} + \frac{\mathrm{Gr}}{\mathrm{Re}^2}\frac{\partial \theta}{\partial X} \tag{15}$$

and applying the nondimensionalization 12 to Equation 7 results in the following:

$$\frac{\partial \theta}{\partial X}\frac{\partial \psi}{\partial Y} - \frac{\partial \psi}{\partial X}\frac{\partial \theta}{\partial Y} = \mathrm{Pr}^{-1}\left\{\frac{1}{\mathrm{Re}^2}\frac{\partial^2 \theta}{\partial X^2} + \frac{\partial^2 \theta}{\partial Y^2}\right\} \tag{16}$$

The coupled nonlinear elliptic Equations 14–16 have now to be solved subject to the following nondimensional boundary conditions:

at

$$X = -b/a\,\mathrm{Re} \quad \text{for} \quad -1 \le Y \le 1 \quad : \psi = Y(3 - Y^2)/2, \; \Omega = 3Y, \; \theta = 0 \tag{17}$$

at

$$Y = -1 \quad \text{for} \quad \begin{matrix} -b/a\,\mathrm{Re} \le X < \infty & : \psi = -1, \; \partial\psi/\partial Y = 0 \\ -b/a\,\mathrm{Re} \le X < 0 & : \theta = 0 \\ 0 \le X < \infty & : \theta = 1 \end{matrix} \tag{18}$$

at

$$Y = 1 \quad \text{for} \quad -b/a\,\mathrm{Re} \le X \le \infty : \psi = 1, \; \partial\psi/\partial Y = 0, \; \theta = 0 \tag{19}$$

at

$$X \to \infty \quad \text{for} \quad -1 \le Y \le 1 \quad : \psi \to Y(3 - Y^2)/2, \; \Omega \to 3Y, \; : \theta \to (1 - Y)/2 \tag{20}$$

for the case of fluid heating from below; i.e., Case I. When the fluid is heated from the upper wall only; i.e. Case II, the thermal conditions in Equation 18 have to be applied at $Y = 1$, the temperature condition in Equation 19 must be applied at the lower wall, $Y = -1$, and the exit temperature profile in Equation 20 replaced by $\theta \to (1 + Y)/2$. Similarly, when the fluid is heated by both walls; i.e., Case III, the thermal conditions for the lower wall in Equation 18 must also be applied at the upper surface, $Y = 1$, and for $X \to \infty$, the asymptotic temperature profile in Equation 20 is replaced by $\theta \to 1$.

Equations 14–16, along with boundary conditions 17–20, are expressed in finite-difference form and an under-relaxation technique is used to solve the resulting algebraic equations on a fine grid (see Ingham et al. 1988a, 1988b, 1990). Furthermore, to satisfy the condition 20, a transformation of the axial coordinate is employed (see Zeldin and Schmidt 1972) for full details). The treatment of the first-order vorticity and temperature derivaties was not originally restricted to the simple first-order upwind scheme that was ultimately used in this study. Central differences produced nonoscillatory solutions for values of $\mathrm{Gr}/\mathrm{Re}^2$ that were sufficiently small. However, for $\mathrm{Gr}/\mathrm{Re}^2 \gg 1$, large gradients, particularly in the vorticity, near any temperature discontinuities resulted in unphysical solutions where spatial oscillations were generated. Second-order upwinding was also rejected, because the range of values of $\mathrm{Gr}/\mathrm{Re}^2$, for a fixed value of Re, for which convergence can be obtained, is smaller than that for the first-order upwind method. Convergence problems of undershoot and overshoot occurred with second-order upwinding; whereas, the QUICK scheme generated unphysical spatial oscillations whenever recirculations were present near the temperature discontinuities.

An absolute convergence criteria was employed; that is, if one additional iteration is performed, then none of the field variables must change by more than a preassigned quantity at any grid point. It was found that a value of 10^{-5} was sufficiently

small so that any further decrease does not change the graphical results presented in this paper. It was found that convergent solutions were only possible if Ω and θ were underrelaxed. Ω more so than θ, and the value of the relaxation parameter for ψ was maintained at unity in every solution. In addition, as the Gr/Re^2 parameter was increased, the relaxation parameters for Ω and θ needed to be decreased.

Results

Results were obtained with 401 × 81, 201 × 41, and 101 × 21 grid points in the stream-wise and transverse directions, respectively. By comparing quantities such as local Nusselt numbers and friction factors it was adequately demonstrated that the grid 201 × 41 was sufficiently fine to obtain accurate solutions; i.e., it is graphically impossible to detect the differences in the results obtained when using the grids 201 × 41 and 401 × 81. Therefore, all the results presented in this paper are those obtained using a grid of 401 × 81. The values of the ratio Gr/Re^2 were chosen as 0, 10, 20, 30, and 40, and the Reynolds number was fixed at 5, 10, and 20, respectively. In addition, the Prandtl number was taken as 7.02, which represents water at 20 C (see Özişik 1985). A variety of stream-wise locations of the duct inlet position were considered, and a value of $-b/a\mathrm{Re} = -0.8$ was chosen, because the velocity and temperature profiles were indistinguishable from the inflow conditions applied as $X \to \infty$.

Situations that involve a hot fluid being cooled by walls maintained at a lower constant temperature can be computed using the model. For example, the main effect of cooling the fluid from below only is that of hydrodynamic and thermal stratification, which is achieved by setting $Gr < 0$. This situation gives rise to flows that are mirror images of the flows presented for the Case II conditions of a hot upper wall only, where $Gr > 0$. The similarity between heating and cooling exists in all three cases and arises because the temperature variable θ appears linearly in the governing Equataions 14–16. Therefore, the results for the cooled wall situations are not presented.

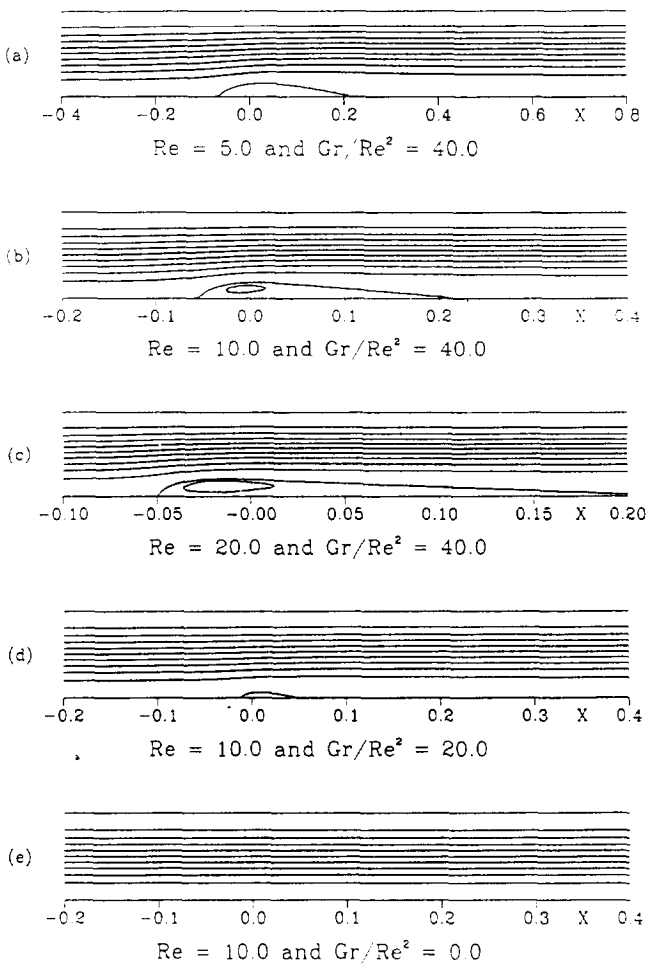

Figure 1 Contour plots of the stream function ψ for the value of Re and Gr/Re^2 indicated for Case I. $\psi \in \{-1.03, -1.0, -0.8, \ldots, 1.0\}$. $\psi = \pm 1.0$ represents the upper (+) and lower (−) walls, respectively

Case I. Heated lower wall

Contours of the nondimensional stream function and temperature for a variety of combinations of Re and Gr/Re^2 are displayed in Figures 1 and 2 respectively, for the case of the fluid being heated by the lower wall. Figures 1a and 2a illustrate clearly the effects of the temperature discontinuity on the lower wall buoyancy-generated recirculation on the fluid and thermal fields. The buoyancy effect is represented by a streamwise temperature gradient in the vorticity transport Equation 15, and hence there exists a mechanism for transportating heat upstream at any value of the Reynolds number. At higher values of Re, streamwise diffusion becomes negligible, and any upstream effects are caused by the buoyancy-generated recirculation. The recirculation region acts as a thermal obstruction, interfering with the passage of heat from the leading edge of the heated surface to the main body of fluid. Thus, the effective duct width is reduced by the presence of the reverse flow region, and this, in conjunction with the continuity of mass principle, causes the downstream section of the flow to experience an increase in streamwise velocity on bypassing the recirulation region.

The effects of increasing the Reynolds number with all remaining parameters held constant are illustrated in Figures 1a–c and 2a–c. The upstream displacement of the separation point increases as the Reynolds number increases. Similarly, the reattachment point moves farther downstream for increasing values of Re. An important difference between Figure 1a–c is how the Reynolds number affects the shape of the recirculation region. The position at which maximum penetration across the duct is achieved by the reverse flow region moves farther upstream as the Reynolds number increases. Figure 2 shows how thermal penetration across the duct improves as Re decreases.

Figures 1b, d, and e as well as 2b, d, and e display how the fluid and thermal fields change with respect to the heating parameter Gr/Re^2 for Re = 10. Forced convection Gr = 0 has the fully developed Poiseuille velocity profile, where changes in temperature have no effect on the fluid density. The dominant processes present are transverse diffusion of heat coupled with its simultaneous advection downstream. Streamwise diffusion does exist and is responsible for the small upstream thermal influence about the onset of heating at the lower wall (see Figure 2e). Computationally, the onset of reverse flow occurs at $Gr/Re^2 \simeq 17$ for Re = 10, and as Re increases, this critical value of Gr/Re^2 slowly decreases. The following general results were observed for increasing values of the parameter Gr/Re^2, with Re fixed.

(1) The size of the recirculation region increases in both the X and Y directions.

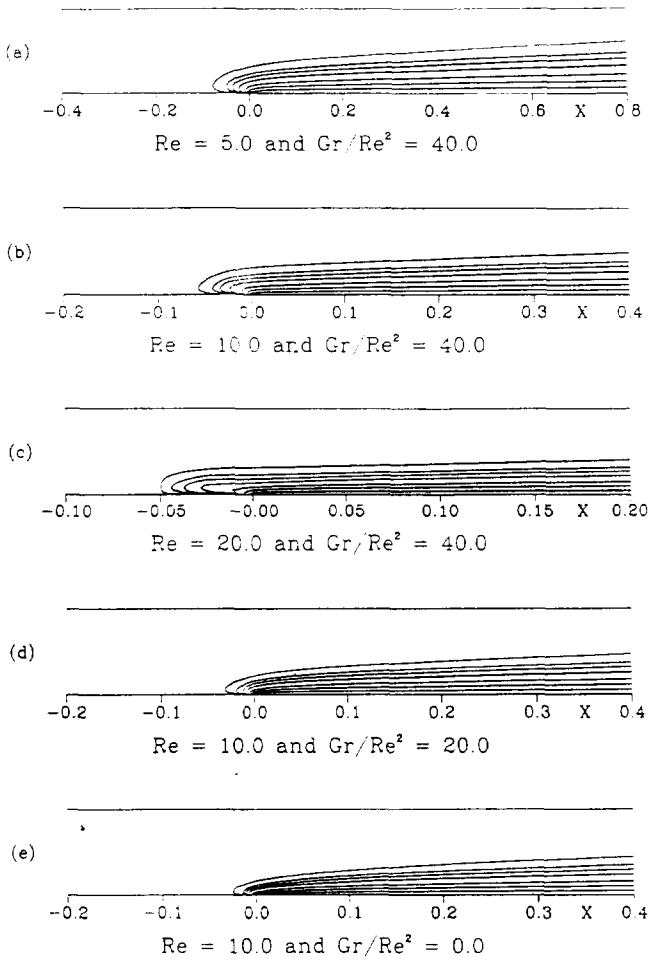

Figure 2 Contour plots of the temperature θ for the value of Re and Gr/Re^2 indicated for Case I. $\theta \in \{0.01, 0.05, 0.1, 0.2, 0.4, 0.6, 0.8\}$ and $\theta = 0.01$ is the contour nearest to the upper wall.

(2) The separation and reattachment points move further upstream and downstream, respectively.
(3) The center of the recirculation is displaced upstream.

The dimensionless bulk temperature θ_m is taken to be the cup mixed temperature, whereby the streams entering a cross section are completely mixed, so that the stream leaving are at an equilibrated temperature. This is essentially an enthalpy balance, and for a recirculation region, it is given by the following equation, which has been rearranged to provide θ_m.

$$\theta_m = \frac{1}{Q_d + Q_u}\left\{\frac{Q_d}{1-A}\int_A^1 \theta\frac{\partial\psi}{\partial Y}\mathrm{d}Y + \frac{Q_u}{1+A}\int_{-1}^{A}\theta\left(-\frac{\partial\psi}{\partial Y}\right)\mathrm{d}Y\right\} \tag{21}$$

where Q_d and Q_u represent the mass fluxes of the downstream and upstream flows within a recirculation region, respectively, and A is the transverse location of the boundary between these flows, which is a minimum turning point in ψ. In the limit of no recirculation, Equation 21 reduces to the normal definition of the dimensionless flow averaged temperature by Shah and London (1978):

$$\theta_m = \frac{1}{2}\int_{-1}^{1}\theta\frac{\partial\psi}{\partial Y}\mathrm{d}Y \tag{22}$$

Equation 21 was chosen to represent the bulk temperature, because this avoided problems with the negative contributions from the upstream traveling fluid to the integral formula Equation 22. The definition 21 will always ensure that the value of θ_m will be positive; although, there may be other definitions for θ_m within the recirculation zone, which will also ensure positive values of the Nusselt number. The dimensionless bulk temperature is plotted as a function of X in Figure 3(a). The upstream transportation of heat caused by the buoyancy-generated recirculation is enhanced as the parameter Gr/Re^2 increases, and this causes the upstream response in θ_m. Thermal penetration across the duct is inhibited by the behavior of the recirculation region, where heat diffused transversely from the lower wall is advected in the upstream direction. This process becomes more dominant as Gr/Re^2 increases, thus producing reduced values of θ_m downstream from the onset of heating. In the limit, as $Y \to \infty$, all the θ_m data curves, for any values of Gr/Re^2 and Re, converge toward the

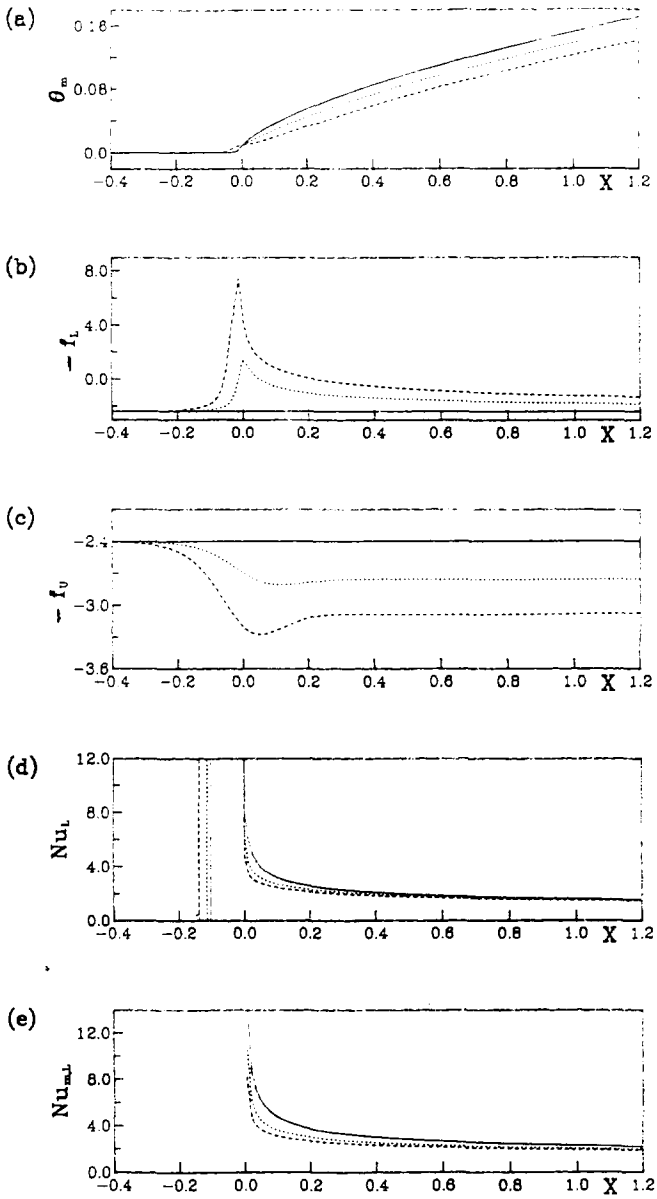

Figure 3 Plots of the bulk temperature, lower wall local and mean Nusselt number, lower and upper wall friction factors for Re = 10 and the values of Gr/Re^2 indicated for Case I. ———, $Gr/Re^2 = 0.0$; . . . , $Gr/Re^2 = 20.0$; – – –, $Gr/Re^2 = 40.0$. The low wall is hotter from $X = 0$ to ∞.

fully developed value of 0.5, as predicted by the classical duct flow situation (see e.g. Shah and London 1978).

The friction factors f for the lower and upper walls are defined (see Özişik 1985) as follows

$$f_L = (-8\Omega|_{Y=-1})\mathrm{Re} \quad : \quad f_U = (+8\Omega|_{Y=1})\mathrm{Re} \tag{23}$$

The friction factors are displayed in Figures 3b and c as a function of X for the lower and upper walls, respectively, for $\mathrm{Re} = 10$ and $\mathrm{Gr}/\mathrm{Re}^2$ in the range [0, 40]. The lower wall values of f peak rapidly at the temperature discontinuity (see Figure 3b). For a fixed value of the Reynolds number, the corresponding wall shear stress eventually becomes negative as the ratio $\mathrm{Gr}/\mathrm{Re}^2$ increases for reverse flow to be initiated. A similar behavior is observed for fixed $\mathrm{Gr}/\mathrm{Re}^2$ as the Reynolds number is increased. The positions of the separation and reattachment points of the dividing streamline that contains the recirculation regions are situated at locations where $f_L = 0$. A change of sign in the wall shear stress indicates a corresponding reversal in the sign of the normal gradient of the local streamwise velocity gradient at the wall. A locally reduced effective duct width at streamwise locations that coincide with the recirculation region coupled with the constant mass flux in the streamwise direction are responsible for the increased upper wall friction factors. The exit flow profile is fully developed, so that for $X \gg 0$, f_L and $f_U \to 2.4$, as predicted by the classical duct flow solution; namely, $f\mathrm{Re} = 24$ (see, e.g., Shah and London 1978).

The local Nusselt numbers become the following:

$$\mathrm{Nu}_L = \left.\frac{\partial\theta}{\partial Y}\right|_{Y=-1} / (\theta_m - \theta|_{Y=-1}) \quad :$$

$$\mathrm{Nu}_U = -\left.\frac{\partial\theta}{\partial Y}\right|_{Y=1} / (\theta_m - \theta|_{Y=1}) \tag{24}$$

for the lower ($Y = -1$) and upper ($Y = 1$) walls, respectively. The lower wall Nusselt number is plotted as a function of the streamwise coordinate X in Figure 3d for $\mathrm{Re} = 10$, and $0 \le \mathrm{Gr}/\mathrm{Re}^2 \le 40$. The temperature field discontinuity is represented by the expected singularity in the local values of Nu_L. Upstream heat transfer effects of the recirculation region produce a rapid increase in the point Nusselt number prior to the onset of heating that occurs at lower values of X as the parameter $\mathrm{Gr}/\mathrm{Re}^2$ is increased for a fixed value of the Reynolds number. Essentially, this is a region where $\partial\theta/\partial Y|_{Y=-1}$ is large and $(\theta_m - \theta|_{Y=-1}) \ll 1$, resulting in numerical values of Nu_L that are greater than 12. Downstream of the onset of heating, successively lower heat transfer coefficients are observed as the value of $\mathrm{Gr}/\mathrm{Re}^2$ is increased for Re in the range [5, 20], which is another consequence of the recirculating region. As $X \to \infty$, the fluid and thermal fields tend to their fully developed states so that $\mathrm{Nu}_L \to 1$, and this is consistent with the classical duct flow results quoted by Shah and London (1978). The upper wall Nusselt numbers remain zero until heat is transmitted across the duct. At some large distance downstream, Nu_U monotonically increases to the classical duct flow solution so that as $X \to \infty$, $Nu_U \to 1$.

The average heat transfer coefficients between the streamwise locations $X = 0$ and $X = L$ is defined as follows:

$$\mathrm{Nu}_m = \frac{1}{L}\int_0^L \mathrm{Nu}\, dX \tag{25}$$

where L is some streamwise location downstream of the onset of heating. Using Simpson's rule to evaluate the integral in Equation 25, then $\mathrm{Nu}_{m,L}$, for the lower wall, is plotted as a function of X in Figure 3e for $\mathrm{Re} = 10$, and $0 \le \mathrm{Gr}/\mathrm{Re}^2 \le 40$. Downstream of the onset of heating, the mean heat transfer coefficients become progressively smaller as the parameter $\mathrm{Gr}/\mathrm{Re}^2$ increases. The largest difference in the average Nusselt numbers occurs within the recirculating region. Within the framework of these purely 2-D flows, the buoyancy-generated recirculation causes advection of heat upstream, resulting in greater removal of heat prior to $X = 0$. Furthermore, the associated backward-moving lower wall layer degrades the heat transfer process for $X > 0$. In comparison to the work of Naito (1984), where entrance region heat transfer coefficients were found to increase at the lower wall in the presence of buoyancy, the present results seem to be contradictory. This difference is probably because of the uniform entry velocity profile used by Naito, where the developing boundary layers immediately downstream of the onset of heating contain shear rates far greater than those associated with development from the Poiseuille entry flow. Hence, the corresponding greater rate of heat advection downstream in the viscous wall layers will enhance the wall heat transfer for $X \ge 0$. In the limit, as $X \to \infty$, all the curves tend to the same limit; namely, $\mathrm{Nu}_{m,L} \to 1$, as expected from the classical duct flow solution (see, e.g., Shah and London 1978).

Case II. Heated upper wall

Contours of the temperature for a variety of combinations of the parameters Re and $\mathrm{Gr}/\mathrm{Re}^2$ are illustrated in Figure 4. The stream function is not displayed, because the effect of buoyancy

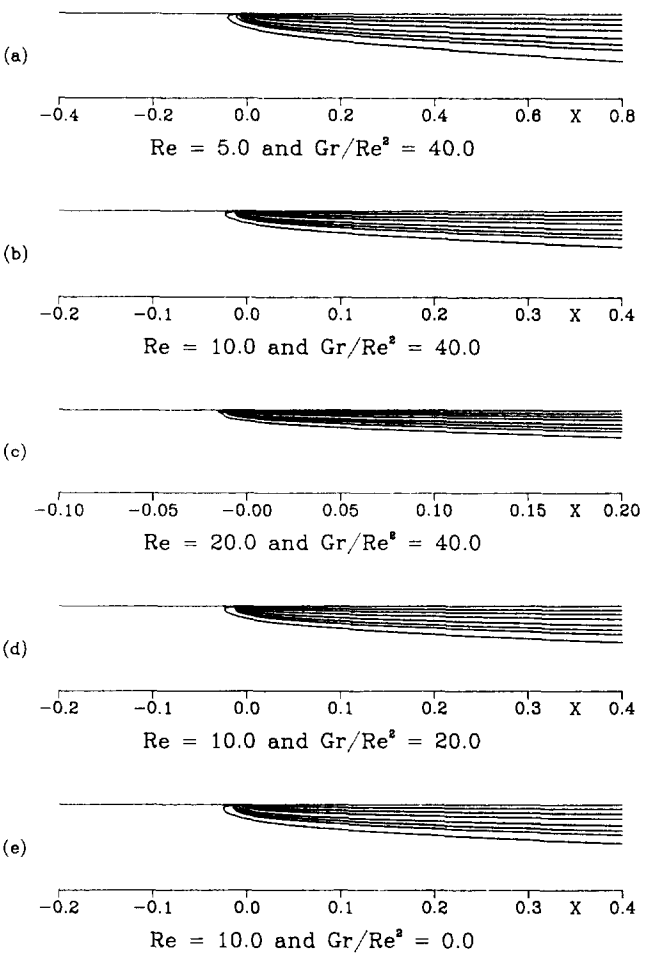

Figure 4 Contour plots of the temperature θ for the values of Re and $\mathrm{Gr}/\mathrm{Re}^2$ indicated for Case II. $\theta \in \{0.01, 0.05, 0.1, 0.2, 0.4, 0.6, 0.8\}$ and $\theta = 0.01$ is the contour nearest to the lower wall.

is simply to produce a stratified layer of heated fluid traveling downstream beneath the upper wall. This type of motion is consistent with the 3-D, finite-difference analysis performed by Incropera and Schutt (1985), where the streamlines tend toward the upper wall near to the onset of heating point, which indicates that within the developing stratified layer, the fluid is accelerated downstream. Consequently, to preserve the mass flux, the streamwise velocities in the entrance region below the heated layer are lower than for fully developed flow. Hence, an effect of developing upper wall stratification is the reduction of the velocity gradients in the vicinity of the lower wall. For a sufficiently high value of Gr/Re^2, the onset and subsequent development of a lower wall recirculation region becomes possible, although no such conditions are considered in this paper. Because any response at the lower wall is caused by upper wall stratification, any such recirculation region generated by heating from above must occur downstream of the onset of the heating location. In the absence of recirculation, the dominant heat transfer process is simply the diffusion of heat from the upper surface, which is then advected downstream. The effect of stream-wise thermal diffusion is illustrated in Figures 4a–c, where the influence upstream of $X = 0$ is reduced as Re increases. In contrast to the previous study for the heated lower wall, the buoyancy effect does not result in the transport of heat and mass upstream, so that as Re becomes large, the solution is of the classical boundary-layer type. The velocity profile returns to the fully developed form, and the temperature gradient across the duct becomes linear as $X \to \infty$.

The dimensionless bulk temperature θ_m as a function of X is displayed in Figure 5a. Because the buoyancy force results in thermal stratification downstream of the onset of heating location, the upstream influence is caused by streamwise diffusion. For Re = 10, increasing the value of the heating parameter Gr/Re^2 leads to greater rates of increase of θ_m about the onset of heating. This trend is maintained downstream so that a larger value of Gr for Re fixed results in stronger thermal stratification, and thus accelerating further the upper wall viscous layer. In all cases, the bulk temperature tends to the theoretical fully developed value of 5.0 as $X \to \infty$, as expected from the classical duct flow solution. Friction factor plots are shown in Figures 5b and 5c as a function of the streamwise coordinate, X for the upper and lower walls, respectively, for $Gr/Re^2 = 0$, 20, and 40, and Re = 10. Except for the forced convection results, where the velocity profile is fully developed everywhere, the upper wall friction factors peak at the onset of heating. Upstream of this location, any deviation from the classical duct flow asymptotic value of $f = 24/Re$ is caused by streamwise diffusion. Hence, as Re becomes large, the upstream effect is reduced, and the velocity profile remains fully developed at all stream-wise locations prior to $X = 0$. Downstream of $X = 0$, the friction factors for values of $Gr/Re^2 > 0$ tend to their asymptotic state.

The upper wall, local Nusselt number as a function of the streamwise coordinate X is shown in Figure 5d for Re = 10, and $0 \le Gr/Re^2 \le 40$. The local Nusselt numbers for $X < 0$ are numerically large, but their associated temperature differences $(\theta_m - \theta|_{Y=-1}) \ll 1$, so that the heat extracted upstream of $X = 0$ at the upper wall is small. In contrast, the heated lower wall results in Figure 3d, show that for $X < 0$, the heat transferred upstream by the buoyancy-induced recirculation strongly dominates that of the streamwise diffusion. The upper wall local Nusselt numbers show a characteristic increase for increasing thermal stratification for $X > 0$. As $X \to \infty$, the asymptotic result for $Nu_U \to 1$ is attained, which is consistent with the predictions for the classical duct flow solution (see Shah and London 1978). In

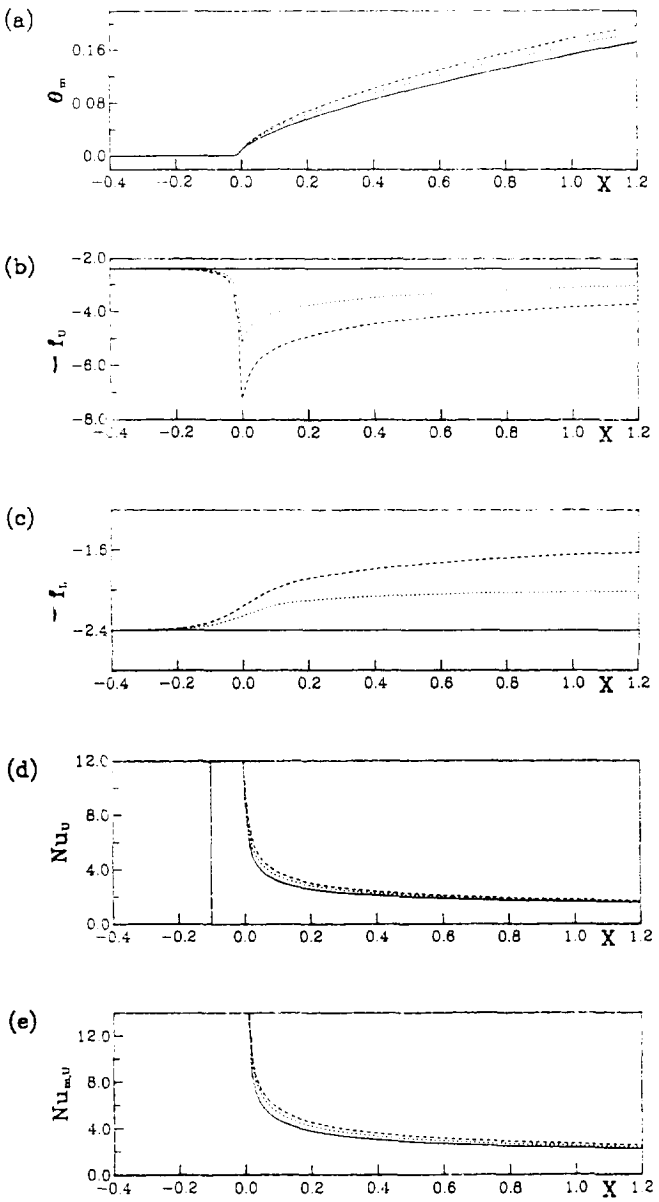

Figure 5 Plots of the bulk temperature, upper wall local and mean Nusselt number, upper and lower wall friction factors for Re = 10 and the values of Gr/Re^2 indicated for Case II. ———, $Gr/Re^2 = 0.0$; . . . , $Gr/Re^2 = 20.0$ – – – $Gr/Re^2 = 40$. The upper wall is hotter from X = 0 to ∞.

this case, plots of the lower wall Nusselt numbers are not shown, because thermal penetration is achieved only at some large distance downstream from the onset of heating; i.e., $Nu_L \ll 1$ in the entrance region, and as $X \to \infty$, increases monotonically toward the fully developed value of unity as predicted by the classical duct flow solution.

The mean upper wall heat transfer coefficients are illustrated in Figure 5e as a function of X for Re = 10 and Gr/Re^2 in the range [0, 40], and they are the integrals of the local Nusselt numbers results in Figure 5d. The main observation is that at any streamwise location downstream of the onset of heating, the average heat transferred through any specified duct wall length increases as the heating parameter Gr/Re^2 increases.

Case III. Heated upper and lower walls

The effect on the fluid and thermal fields of enforcing temperature discontinuities at the same streamwise location on both walls is to bring together all the individual characteristics of the Cases I and II and enhance them. The reduction of the lower wall shear stresses by upper surface thermal stratification certainly enlarges the recirculation region on the lower wall by moving the reattachment point a significant distance downstream. Upper wall conditions also influence the upstream separation point, which is displaced further upstream, and the depth of penetration across the duct, which also increases. Fluid that bypasses the recirculation region is accelerated through the reduced duct width, and the increased velocity gradients in the vicinity of the upper wall lead to increased advection of heat downstream and greater thermal stratification. The results obtained by varying Re for Gr/Re^2 fixed, or fixing Re and changing Gr/Re^2, remain broadly as described in the studies for the heating of a single wall.

It has already been shown that the lower wall recirculation region reduces the heat transfer rates to below those of forced convection. Hence, when both walls are heated, and the reverse flow region is enlarged, then heat extracted by the upstream section ($X < 0$) of the lower wall is increased, and the heat transferred to the recirculation is reduced at each streamwise location for $X > 0$. The reverse effect occurs at the upper wall where more powerful stratification leads to greater heat transfer. The basic form of the friction factors is not significantly different by the single-wall heated cases, but at each streamwise location, the actual deviation from the fully developed value is greater. Figure 6 contains plots of the bulk temperature, the wall shear stresses for both walls, and the upper and lower wall average Nusselt numbers.

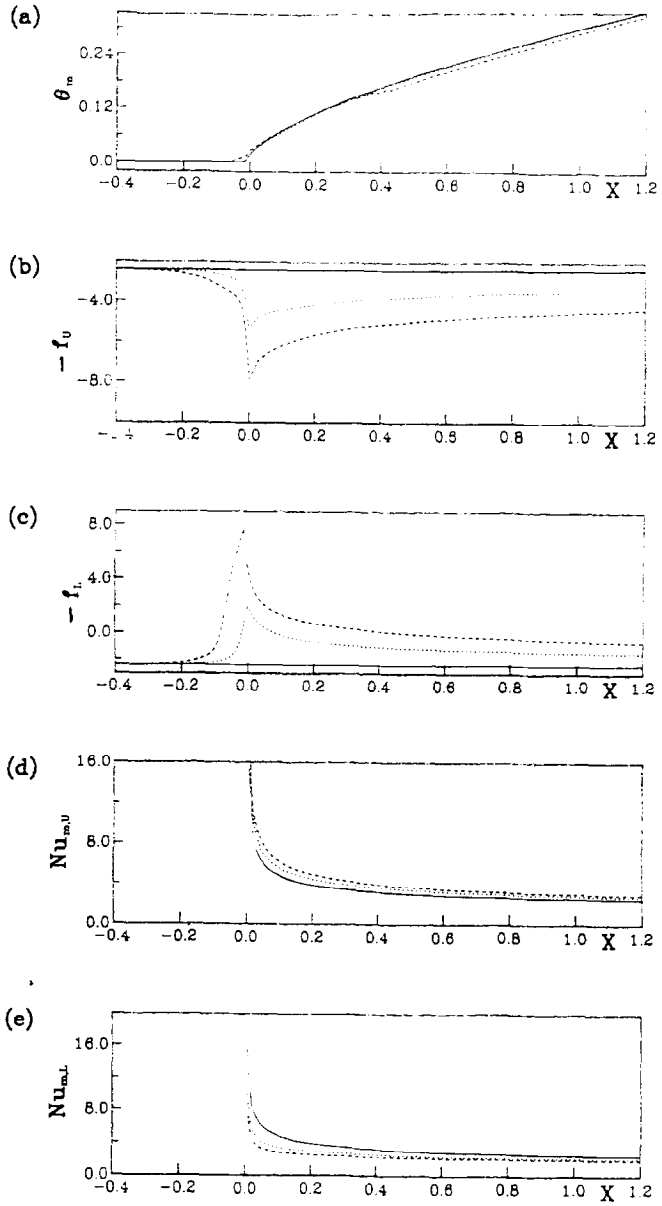

Figure 6 Plots of the bulk temperature, upper and lower wall mean Nusselt number, upper and lower wall friction factors for Re = 10, and the values of Gr/Re^2 indicated for Case II. ——— $Gr/Re^2 = 0.0$ ··· $Gr/Re^2 = 20.0$ – – – $Gr/Re^2 = 40.0$ both walls are hotter from X = 0 to ∞.

Conclusions

The numerical results of Case I illustrates how a buoyancy-generated lower wall recirculation region significantly changes the heat transfer process. The mechanism of thermal diffusion from a hot surface and its advection downstream associated with forced convection is replaced about $X = 0$ by diffusion of heat into a slow recirculating region, which is then transported upstream of the thermal discontinuity, allowing heat to be extracted from the fluid. Within the reverse flow region, a heated viscous wall layer moves upstream, which results in a weaker thermal gradient, and thus reduces the heat transferred at the lower wall in the entrance region, as compared to that obtained for purely forced convection.

The heat transfer process at the upper wall in Case II is aided by buoyancy, which generates a thermally stratified upper wall layer, and a large thermal gradient exists across this thin viscous wall layer, thus enhancing the entrance region heat transfer. If the thermal stratification is sufficiently powerful, a lower wall recirculation region will be created downstream of the onset of heating location. Parameter values for Re and Gr/Re^2 can be found that indicate that this, as yet unobserved, steady laminar flow should exist.

The Case III results illustrate how the recirculation and stratification effects of the Cases I and II are combined and enhanced. In particular, an effect of lower wall recirculation is to generate a compressed viscous upper wall layer that aids the stratification process. The thermally stratified upper wall layer has been shown to induce lower wall recirculations and will, therefore, strengthen and enlarge an existing lower wall recirculation region. The separation and reattachment lengths are greater in Case III than in Case I, and the lower wall heat transfer in Case III is poorer than in Case I because of greater recirculation effects. The upper surface heat transfer in case III is greater than in Case II because of increased stratification. A stability analysis of the above flows is now under way.

References

Akiyama, M., Hwang, G. J. and Cheng, K. C. 1971. Experiments on the onset of longitudinal vortices in laminar forced convection between horizontal plates. *J. Heat Transfer*, **93**, 335–341

Aung, W. 1987. *Mixed Convection in Internal Flow*. In *Handbook of Single-Phase Convective Heat Transfer*. S. Kakaç et al. (eds.), Wiley, New York, chapt. 15

Collins, M. W. 1975. Viscous dissipation effects on developing laminar flow in adiabatic and heated tubes. *Proc. Inst. Mech. Eng.*, **189**, 129–137

Collins, M. W. 1980. Finite difference analysis for developing laminar flow in circular tubes applied to forced and combined convection. *Int. J. Num. Meth. Eng.*, **15**, 381–404

Incropera, F. P. and Schutt, J. A. 1985. Numerical simulation of laminar mixed convection in the entrance region of horizontal rectangular ducts. *Num. Heat Transfer*, **8**, 709–729

Ingham, D. B., Keen, D. J. and Heggs, P. J. 1988a. Two-dimensional combined convection in vertical parallel plate ducts, including situations of flow reversal. *Int. J. Num. Meth. Eng.*, **26**, 1645–1664

Ingham, D. B., Keen, D. J. and Heggs, P. J. 1988b. Flows in vertical channels with asymmetric wall temperatures and including situations where reverse flows occur. *J. Heat Transfer*, **110**, 910–917

Ingham, D. B., Keen, D. J., Heggs, P. J. and Morton, B. R. 1990. Recirculating pipe flows. *J. Fluid Mech.*, **213**, 445–464

Mori, Y. and Uchida, Y. 1966. Forced convection heat transfer between horizontal flat plates. *Int. J. Heat Mass Transfer*, **9**, 803–817

Morton, B. R., Ingham, D. B., Keen, D. J. and Heggs, P. J. 1989. Recirculating combined convection in laminar pipe flow. *J. Heat Transfer*, **111**, 106–113

Naito, E. 1984. Buoyant force effects on laminar flow and heat transfer in the entrance region between horizontal parallel plates. *Heat Trans. Jap. Res.*, **13**, 80–96

Naito, E. and Nagano, Y. 1989. Combined forced and free upward-flow convection in the entrance region between inclined parallel plates. *J. Heat Transfer*, **111**, 675–682

Nakayama, W., Hwang, G. J. and Cheng, K. C. 1970. Thermal instability in plane Poiseuille flow. *J. Heat Transfer*, **92**, 61–68

Osborne, D. G. and Incropera, F. P. 1985. Laminar mixed convection heat transfer for flow between horizontal parallel plates with asymmetric heating. *Int. J. Heat Mass Transfer*, **28**, 207–217

Özişik, M. N. 1985. *Heat Transfer, A Basic Approach*, McGraw-Hill, New York

Shah, R. K. and London, A. L. 1978. *Advances in Heat Transfer, Supplement 1, Laminar Flow Forced Convection in Ducts*. Academic Press, San Diego

Zeldin, B. and Schmidt, F. W. 1972. Developing flow with the combined forced-free convection in an isothermal vertical tube. *J. Heat Transfer*, **94**, 211–223